Effect of ingested tungsten oxide (WOX) nanofibers on digestive gland tissue: Synchrotron-based Fourier transform infrared (FTIR) microspectroscopy

SCHOLARONE™
Manuscripts

Model organism

Tungsten oxide nanofibers

Model digestive tissue (hepatopancreas)

Nanofiber trusted in cell

Optical and Fourier transform infrared (FTIR) image of digestive tissue

Partial reorganization of the nucleic acid structure

Average spectra of control (black line) and nanofiber exposed (red line) of digestive tissue in nucleics acids region
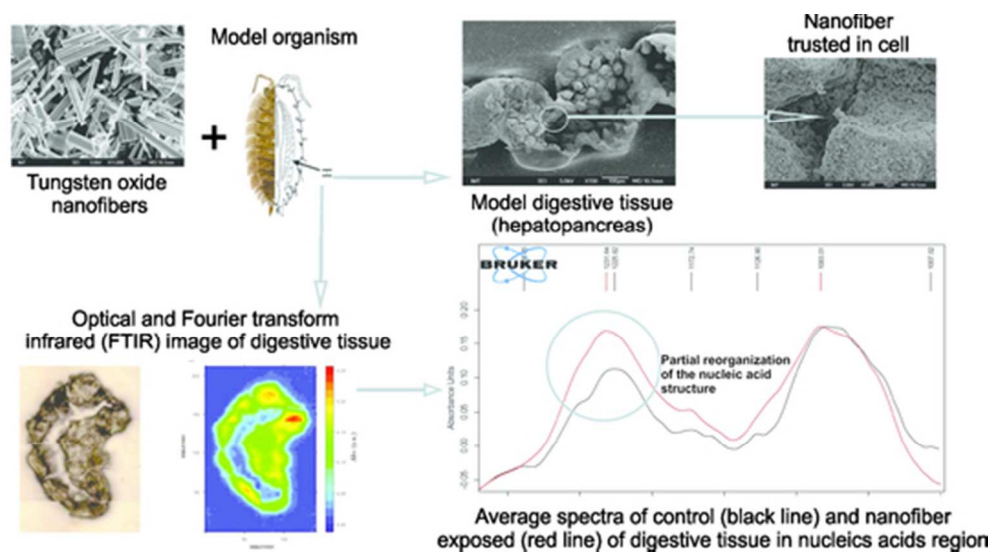
46x24mm (300 x 300 DPI)

Effect of ingested tungsten oxide (WO$_X$) nanofibers on digestive gland tissue: Synchrotron-based Fourier transform infrared (FTIR) microspectroscopy

Sara Novak[‡], Damjana Drobne[‡,§,†,*], Lisa Vaccari[¶], Maya Kiskinova[¶], Paolo Ferraris[¶], Giovanni Birarda[▢], Maja Remškar[¥], Matej Hočevar[▢]

[‡]Department of Biology, Biotechnical Faculty, University of Ljubljana, Ljubljana, Slovenia,

[§]Centre of Excellence, Advanced Materials and Technologies for the Future (CO NAMASTE), Ljubljana, Slovenia,

[†]Centre of Excellence, Nanoscience and Nanotechnology (Nanocentre), Ljubljana, Slovenia,

[¶]Elettra-Sincrotrone Trieste, AREA Science Park, Basovizza, Trieste, Italy,

[▢] Lawrence Berkeley National Laboratory, 1 Cyclotron Rd. Berkeley CA, USA,

[¥]Jožef Stefan Institute, Condensed Matter Physics Department, Jamova cesta 39, 1000 Ljubljana, Slovenia,

[▢]Institute of Metals and Technology, Lepi pot 11, 1000 Ljubljana, Slovenia

* Corresponding author: damjana.drobne@bf.uni-lj.si

1

1 **Abstract**

2 Tungsten nanofibers are recognised as biologically potent. We study deviations in molecular

3 composition between normal and digestive gland tissue of WO_x nanofibers (nano-WO_x) fed

4 animals and reveal mechanism of nano-WO_x effect on digestive gland cells of a model

5 organism *in vivo*. Fourier transform infrared (FTIR) spectroscopy was performed on digestive

6 gland epithelium of animals fed with WO_x nanofibers. The FTIR analyses were supplemented

7 by toxicity and cytotoxicity analyses as well as scanning electron microscopy (SEM) of the

8 surface of the epithelium. The difference in the spectra of the WO_x-treated and control cells

9 showed up in the central region of the cells and are related to a changed protein to lipid ratio,

10 lipid peroxidation and structural changes of nucleic acids. The conventional toxicity

11 parameters failed to show toxic effects of nano-WO_x, whereas the cytotoxicity biomarkers and

12 SEM investigation of digestive gland epithelium indicate sporadic effects of nanofibers. The

13 FTIR results are in agreement with toxicological and cytological measurements, which

14 indicate that ingestion of nano-WO_x does not affect severely the cell membrane stability and

15 feeding behaviour. However, we explain changes observed by FTIR as protection of cells to

16 unfavourable conditions and indication of non-homeostatic state, which can lead to toxic

17 effects.

18

19

20

21

22

23

2

Introduction

24

25   Tungsten oxides (WO_3, WO_2, and WO_x), which have attractive semiconductor

26 properties, have been considered for many important applications including optical devices,

27 gas sensors, electrochromic windows, and photocatalysts.[1] Synthesis of tungsten oxides

28 however can be accompanied by release of fiber-like nanoparticles which raises safety

29 concerns reminiscent of those associated with asbestos fibers, which were found to be highly

30 toxic inducing irreversible health problems.[2]

31   Exposures to tungsten and its compounds in occupational environments include those

32 during production of tungsten metal from the ore and fabrication of tungsten carbide powders

33 in the tungsten refining and manufacturing industry (Agency for Toxic Substances and

34 Disease Registry, 2005). WO_x nanofibers, whiskers or needles are recognised as being more

35 biologically potent than non-fibrous WO_x due to their ability to produce free radical damage

36 *in vitro.*[3] Tungsten carbide particles (WCs) that can cause pneumoconiosis[4] are also well

37 known.

38   Detection of biological effects can be gained from comparisons of healthy and

39 abnormal tissue, what can be carried out by a variety of physical, biological and biochemical

40 methods. The selection of methods is based on the expected alteration but, when it is

41 necessary to shed more light on molecular and functional changes, methods which can

42 monitor a broad range of structural or functional alterations are required. Among these,

43 Fourier Transform InfraRed (FTIR) microspectroscopy which uses IR radiation to detect

44 deviations in molecular composition between normal and abnormal tissue is very promising.[5]

45 This technique is based on absorption of infrared light by the vibrational transitions in

46 covalent bonds and intensities provide quantitative information, while frequencies give

47 qualitative information about the nature of these bonds, their structure, and their molecular

3

48   environment. FTIR microspectroscopy is a label-free, non-destructive and objective tool for

49   discriminating between normal tissues and any alteration. In complex systems such as cells,

50   the main spectral features arise from N-C=O, N–H, C=O, C–H and P=O bonds in proteins,

51   lipids, and nucleic acids. The infrared spectrum of cells reflects all these contributions and

52   provides information on the concentration, organization and structure of the most fundamental

53   macromolecules.[6]

54   Interactions between cells and nanoparticles lead to alteration in cell metabolism,

55   activation of mechanisms that protect against oxidative stress, toxic response and finally cell

56   death.[7,8] Many papers report effects of nano and microparticles on lipid and protein

57   oxidation,[9,10,11] changes in cell membrane fluidity,[9] alterations of proteins[10,11] and of DNA.[5]

58   The aim of our work was to study deviations in molecular composition between

59   normal digestive gland tissue and digestive gland tissue of WO_x nanofibers (nano-WO_x) fed

60   animals and reveal mechanism of nano-WO_x effect on digestive gland cells of a model

61   organism *in vivo*.

62   The model organism we used was a terrestrial invertebrate *Porcellio scaber* (Isopoda,

63   Crustacea). The advantage of using this organism is the possibility of directly correlating the

64   actual exposure dose to nanofibers and observed effects at different levels of biological

65   organization. The feeding parameters are an integrated organism-level response, appropriate

66   evidence of the effects of different chemicals at organism level.[12,13] Cellular and biochemical

67   analyses indicate cell level evidence after exposure to chemicals or nanoparticles and to a

68   certain degree their mode of action. Digestive gland cells (hepotopancreas) of terrestrial

69   isopods which combine the functions of pancreas and liver in vertebrates are preferred tissue

70   to study effects of substances with unknown and untargeted action in digestive system.

4

71   In this study we used FTIR microspectroscopy to study the type and level of digestive

72   gland cell alterations due to ingestion of WO_x nanofibers. It was expected that comparison of

73   the FTIR spectra of control and nano-WO_x-fed test animals will indicate the biological

74   consequences of ingestion of nanofibers.

75

Experimental

77   **Chemicals**

78   Acridine orange (AO), ethidium bromide (EB), sodium chloride (NaCl), potassium

79   chloride (KCl), magnesium chloride ($MgCl_2$), glucose and 2-amino-2-hydroxymethyl-

80   propane-1,3-diol (TRIS), were purchased from Merck. Cobalt (II) chloride hexahydrate

81   ($CoCl_2.6H_2O$), 99.9% (metal basis) was purchased from Alfa Aesar Johnson Mathey

82   Company. The WO_x nanofibers were synthesized at Jozef Stefan Institute, Condensed Matter

83   Physics Department. Tungsten powder (99.9%), WO_3 powder (99.9%) and Iodine (99.8%)

84   were purchased from Sigma-Aldrich.

85   **Model organisms**

86   Terrestrial isopods (*Porcellio scaber,* Isopoda, Crustacea) were collected during July

87   2010 at an uncontaminated location near Ljubljana, Slovenia. The animals were kept in a

88   terrarium filled with a layer of moistened soil and a thick layer of partly decomposed hazelnut

89   tree leaves (*Corylus avellana*), at a temperature of 20 ± 2 °C and a 16:8-h light:dark

90   photoperiod. Only adult animals of both sexes and weighing more than 30 mg were used in

91   the experiments. If moulting or the presence of marsupia were observed, the animals were not

92   included in the experiment in order to keep the investigated population physiologically as

93   homogenous as possible.

5

94   The digestive system of the terrestrial isopod *P. scaber* is composed of a stomach, four

95   blind-ending digestive gland tubes (hepatopancreas) and a gut. Food enters the digestive

96   glands directly *via* a short stomach or after the reflux from the gut and ingested material is

97   mixed with digestive fluids.

98   **Synthesis and characterization of WO_x nanofibers**

99   The WO_x nanofibers were synthesized by a chemical transport reaction[14] from

100   tungsten powder (99.9%) and WO_3 powder (99.9%) in the stoichiometric ratio of $WO_{2,86}$.

101   Iodine (99.8%) in a volume fraction of 3.2 mg/cm^3 was added as a transport agent. The

102   material was transported from the source (hot zone at 1123 K) to the growth zone (1009 K),

103   with a 5.7 K/cm temperature gradient. The produced nanofibers were studied using electron

104   transmission microscopy 200 keV Jeol 2010F, scanning electron microscopy (FE-SEM, Supra

105   35 VP, Carl Zeiss). XRD spectra were recorded with an AXS D4 Endeavor diffractometer

106   (Bruker Corporation, Karlsruhe,Germany), with Cu Ka1 radiation and a SOL-X energy

107   dispersive detector with the angular range of 2θ from 5° to 75°, a step size of 0.04° and a

108   collection time of 3 to 4 s.

109   **Food preparation**

110   In this study the animals consumed particles applied in a suspension to the leaf

111   surface. Hazelnut leaves were collected in an uncontaminated area and dried at room

112   temperature. Dried leaves were cut into pieces of approximately 100 mg. The WO_x nanofibers

113   were suspended in distilled water before each experiment to obtain the final concentration of

114   5000 µg nano-WO_x/ml. To diminish agglomeration of nanofibers in distilled H_2O the

115   suspension was sonicated in an ultrasonic bath for 1h and mixed using a vortex mixer before

116   brushing it on the leaves. In the control group, the leaves were treated only with distilled

117   water. The suspension of nanofibers or the distilled water was brushed onto the abaxial leaf

6

118 surface to give final nominal concentrations of nanoparticles on the leaves of 5000 µg nano-

119 WO_x per gram (dry wt) of leaf and left until dry.

Experimental setup

121 Each individual animal was placed in a 9 cm Petri dish. A single hazelnut leaf segment

122 treated with distilled water or nano-WO_x suspension (5000 µg/g of WO_x) and placed in each

123 Petri dish was the animal's only food source. Humidity in the Petri dish was maintained by

124 spraying tap water on the internal side of the lid every day. All Petri dishes were kept in a

125 large glass container under controlled conditions in terms of air humidity ($\geq 80\%$), temperature

126 ($21\pm1°C$) and light regime (16:8h light: dark photoperiod). After the exposure, the animals

127 were anaesthetized at low temperature and then decapitated and their digestive glands isolated

128 and subsequently used for different analyses.

Feeding parameters, weight change and survival

130 After 7 days of exposure of the animals to treated leaves, the faecal pellets and leaves

131 were removed from the Petri dishes, dried at room temperature for 24 h and weighed

132 separately. The feeding rate of isopods was calculated as the mass of leaves consumed per

133 animal's wet weight per day. The food assimilation efficiency was calculated as the difference

134 between the mass of consumed leaves and mass of faecal pellets divided by the mass of

135 consumed leaves. The weight change of an animal was the difference in its mass from the

136 beginning to the end of the experiment.

Digestive gland cell membrane stability assay

138 The cell membrane stability was tested with the modified method previously described

139 by Valant et al.[15] A single isolated hepatopancreatic tube was incubated for 5 min in a mixture

140 of the fluorescent dyes acridine orange and ethidium bromide and then put on a microscope

141 slide. Fresh samples were examined by an Axioimager.Z1 fluorescent microscope (Zeiss) and

7

142 photographed with two different sets of filters. The excitation filter 450 to 490 nm and the

143 emission filter 515 nm (filter set 09) were used to visualize AO and EB stained nuclei, while

144 the excitation filter 365 nm and the emission filter 397 nm (filter set 01) were used to

145 visualize nuclei stained with EB only. The cell membrane integrity was assessed by

146 examination of the micrographs. Photographs of intact digestive glands were examined by the

147 same observer twice at intervals of at least 24h. The integrity of cell membrane was assessed

148 visually and classified on the basis of a predefined scale from 0 to 9. From preliminary

149 experiments, it was concluded that the non-treated (control) animals show <5% of nuclei

150 stained by EB, while severely stressed animals have up to 100% of EB-stained nuclei. The

151 <5% of hepatopancreatic tubes stained with EB were classified as 0, and those with the

152 highest proportion (>95%) of EB stained nuclei as 9.[15] Our previously published results have

153 demonstrated that in animals in good physiological condition from a stock culture, the

154 digestive gland cell membrane stability value was higher than 2 in only 5% of animals and

155 this was taken as a benchmark. [15] The cell membranes are considered to be destabilised when

156 the value is higher than 2.

157 **FTIR imaging**

158 For FTIR imaging, digestive glands were shock-frozen in liquid N_2, using tissue-

159 freezing medium (Jung Tissue Freezing Medium, Leica). 15 µm thick samples were sectioned

160 using a Leica CM3050 cryotome with the temperature of the microtome head and chamber

161 maintained between -25 °C and -20 °C. The sections were then placed onto CaF_2 IR

162 transparent windows 2 mm thick.

163 FTIR measurements were carried out at the infrared beamline SISSI (Synchrotron

164 Infrared Source for Spectroscopy and Imaging) of Elettra Synchrotron laboratory[16] using the

165 Vertex 70 interferometer coupled with Hyperion 3000 Vis-IR microscope. Both the

166 interferometer and microscope were purged with N_2. The IR images were acquired in

8

167   transmission mode using the bidimensional Focal Plane Array (FPA, 64X64 pixel) detector,

168   averaging 256 scans per spectrum. Each FPA image is composed by 4096 spectra and by

169   using a 15X condenser/objective (NA=0.4), a ~170X170 μm^2 sample area was imaged

170   achieving a pixel resolution of about 2.6 µm. Each image was pre-processed by running the

171   atmospheric compensation routine of OPUS 6.5 (Bruker Optics GmbH, Ettlingen, Germany)

172   in order to minimize spectral contributions from water vapour and carbon dioxide. The

173   simpler FTIR image is generated by integrating a specific spectral band or a spectral region

174   for each image pixel, following *univariate analysis*. The integration results are then plotted in

175   2D using a colour scale and providing information on the distribution of a functional group

176   within the sample, and consequently of the bio-macromolecules that contain it (Figure S1A,B,

177   Supporting Information). Figure S1B (Supporting Information) was obtained following this

178   procedure, integrating the 1720-1480 cm^{-1} spectral region, which contains the most intense

179   bands of cellular proteins, Amide I and II (Table S1, Supporting Information). The spectral

180   band assignment was done in accordance with published recommendations (listed in Table

181   S1, Supporting Information). The spectral bands relevant for this manuscript and their

182   assignment are reported in Table S1, Supporting Information.

183   Penetration of the tissue-freezing medium (TFM) into the sample is usually minimal

184   and dependent on the tissue type.[17,18] Typically, the TFM could be detected as an additional

185   thin layer surrounding the tissue. However, the TFM penetration within the sample was

186   presumed to be different between different specimen regions and among samples, depending

187   also upon dragging effects during cutting. Figure 1 shows the spectra of the tissue freezing

188   medium (black dotted line), of a peripheral and central point of the sample control K2, black

189   and grey continuous lines, respectively. In particular, a strong and sharp tissue freezing

190   medium peak centred at 1116 cm^{-1} could affect the spectral profile below 1200cm^{-1}. The Jung

191   TFM has vibrational features that overlap with some characteristic spectral bands can impose

9

192   some limitation to the diagnostic potentials of the technique: its contribution is clearly visible

193   in the peripheral region spectrum (black continuous line) while it is not detectable in the

194   central part of the same sample. Consequently, a procedure was developed for subtraction of

195   the TFM contribution from the sample vibrational pattern.

196   We developed a chemometric approach based on the HyperSpecJSS program

197   (http://hyperspec.r-forge.r-project.org).[19,20] The routine steps are presented schematically in

198   Figure 2 for the control sample K1 (see optical image 2 A) and listed as follows: i)

199   Hierarchical Cluster Analysis (HCA), Euclidean distances & Wards' algorithm on absorbance

200   spectra was carried out in the spectral region 1720-1480 cm^{-1} (FTIR image of protein

201   distribution in Figure 2 B) and the cluster centroid of the freezing medium was identified. It

202   corresponds with the sampled region outside the specimen, black in Figure 2C, ii) The tissue

203   freezing medium distribution was evaluated by integrating the characteristic tissue freezing

204   medium band centred at 1116 cm^{-1} as height integral (Figure 2 D).The integral intensities over

205   the image were normalized to 1 in order to generate the matrix of subtraction coefficients. iii)

206   The TFM spectrum was subtracted pixel by pixel from the sample spectrum by applying the

207   subtraction coefficients obtained in the previous step. The procedure was repeated twice per

208   sample (Figures 2 E, F).

209   Images corrected for the TFM contribution were analysed independently in order to

210   highlight the biochemical diversity between central and peripheral sample regions. The

211   aforementioned regions have been discriminated against by applying HCA in the spectral

212   region 3050-2800 cm^{-1} on vector normalized absorbance spectra (Euclidean distances &

213   Wards' algorithm). Comparing optical and FTIR images, it was deduced that apical and basal

214   parts of the epithelium represent the peripheral, while the central part of epithelium, located

215   around nuclei formed the central region (Figure 2 I). More than 6000 spectra, divided between

10

216   peripheral and central regions, have been selected and further analysed following the

217   procedure described above.

Scanning electron microscopy (SEM) and Energy dispersive X-ray analysis (EDX)

219   After the feeding experiment, animals were decapitated and the hepatopancreas was

220   isolated and immediately transferred with tweezers to the fixative containing 2.5%

221   glutaraldehyde, 0.4% paraformaldehyde and 0.1M sodium phosphate buffer (pH 7.2). After

222   primary aldehyde fixing, digestive glands were put in 1% osmium tetroxide and stained with

223   TOTO   (thiocarbohydrazide/osmiumtetroxide/thiocarbohydrazide/osmiumtetroxide)

224   conductive, a method previously described by Leser et al.[21] The fixed hepatopancreas glands

225   were dehydrated in absolute alcohol and dried with hexamethyldisilizane (HMDS). The dry

226   samples were mounted on holders and sputter coated with gold-palladium (Sputter coater

227   SCD 050, BAL-TEC).

228   Samples were investigated by field emission scanning electron microscopy (SEM; Jeol

229   JSM-6500F, at the Institute of Metals and Technology in Ljubljana). Energy dispersive X-ray

230   analysis (EDX) was used to analyse the chemical composition of selected parts of the

231   epithelial surface (EDX/WDX Oxford Instruments INCA, Jeol JSM-6500F, at the Institute of

232   Metals and Technology).

Data analysis

234   Data were analyzed by standard statistical methods. The difference in the median

235   measured parameters in exposed and unexposed groups was tested with the non-parametric

236   Mann-Whitney U test. All calculations were performed with Statgraphics Plus 4.0.

237

238

11

Results

Characterization of WO_x nanofibers

The WO_x fibers were grown as single crystalline fibers with high aspect ratio (Figure 3A). While their diameter typically did not exceed 100 nm, their length was on the millimetre scale. An electron diffraction pattern taken on a single fiber (Figure 3B) corresponds to the W18O49 phase. The $[1\bar{2}1]$ zone axis is shown. X-ray diffraction confirms the monoclinic W18O49 phase (JCPDS-71-2450). Impurities of other WO_x phases are possible with quantities below the detection limit of 2-3 %.

Feeding parameters, weight change and survival

Weight, survival and feeding parameters were not affected when animals were exposed to leaves dosed with WO_x nanofiber suspension, providing nominal concentrations of 5000 µg nano-WO_x/g of leaf.

Digestive gland cell membrane stability assay

In control group, 90% of animals had a cell membrane stability of, nominally 2 (Figure 4). In 10% of exposed animals, it was slightly higher and assigned the value 3. We ascribe this to suboptimal experimental conditions.

In animals fed on food dosed with nano-WO_x the stability of the digestive gland cell membrane was affected in almost 20% of animals, while 10% of them had severely affected cell membranes (Figure 4).

FTIR imaging

The average spectra of peripheral and interior regions for each sample as obtained from HCA have been compared by verifying their spectral similarities. In particular, we

12

261   analysed differences between control and exposed samples in the peripheral region, the apical

262   part of the digestive gland epithelia, and between controls and exposed samples in the central

263   part of the epithelia, which is the region between the apical and the basal layer of the cells.

264   The analysis did not highlight any significant differences between the control and nano-WO_x

265   treated peripheral regions that are also those mostly affected by tissue freezing medium

266   penetration. In contrast, following nanoparticle ingestion noticeable biochemical alterations

267   were found in the internal sectors.

268   Figures 5A, B show the average spectra of central parts of the WO_x and control

269   samples, as obtained upon standard vector normalization on the 3000-2800 cm^{-1} range. In

270   order to highlight compositional modification affecting the samples following ingestion of

271   WO_x NPs, several spectral regions have been integrated. Since inhomogeneity in the sample

272   thickness, both within and between samples, can affect the integral values, integral ratios have

273   been considered. Second derivatives of average spectra are shown in Figures 5C, D, and have

274   been considered for highlighting structural differences among the samples.

275   The ratio of area integrals between 1720-1480 cm^{-1} and 3000-2800 cm^{-1} decreased

276   significantly upon ingestion of nanofibers, from 3.536±0.033 to 2.1563±0.221, revealing a

277   remarkable decrease in the protein to lipid content (Table S1, Supporting Information).

278   However, no significant differences in either relative intensity or energy were detected for

279   methyl and methylene stretching bands. Asymmetric and symmetric -CH_3 and -CH_2 stretching

280   bands were found at 2960±2, 2873±2, 2925±2 and 2852±2 cm^{-1}, respectively, in both control

281   and treated samples and their integral height ratio did not change upon treatment. Conversely,

282   an upshift of both vinyl (3007 - 3012 cm^{-1}) and methine (2893 - 2896 cm^{-1}) moieties was

283   evident upon treatment of nanofibers, followed by the downshift of the carbonyl ester

284   stretching band from 1743 to 1739 cm^{-1}. No protein structural variations were detected upon

285   nano-WO_x ingestion. Amide I and Amide II components remained constant and contribution

13

286 from α-helix (AmI, 1660 cm^{-1}; AmII, 1545 cm^{-1}), random coil (AmI, 1640 cm^{-1}) and β-sheet

287 (AmI, 1688/1613 cm^{-1}) structures were found for both control and nano-WO$_x$ treated samples.

288   The asymmetric bending mode of methyl groups and the deformation of methylene

289 moieties was centred at 1457 cm^{-1} in control samples, while the methylene (υ $_{asym}$CH$_3$,

290 1464cm^{-1}) and methyl (υ CH$_2$, 1453cm^{-1}) contributions could be distinguished in WO$_x$ treated

291 samples. The symmetric bending mode of methyl groups reflected the former trend, splitting

292 from 1394 to 1382 and 1399 cm^{-1} upon ingestion of NPs. The ratio of the bands centred at

293 ~1740 and ~1464 cm^{-1} is much higher for treated samples (0.692±0.105) than for the controls

294 (0.378±0.069). The ratio between ~1464 to ~1400 cm^{-1} changed from 0.600±0.062 to

295 1.187±0.057. The asymmetric phosphate band had 2 major components, centred at 1217 and

296 1232 cm^{-1} in both control and treated samples, but the former became much weaker upon

297 treatment.

298 **Scanning electron microscopy (SEM) and Energy dispersive X-ray analysis (EDX)**

299   Digestive glands of animals fed with food dosed with 5000 µg nano-WOx/g of food

300 were prepared for scanning electron microscopy. Fiber-like structures were observed on the

301 surface of some cells of digestive glands (Figure 6A). We analysed these structures with EDX

302 and the chemical composition reveals the presence of tungsten (Figure 6B, C).

303   In 25% of animals these irregularly shaped structures were found to be thrust into the

304 cells. Such structures have never been found in control animals or observed during our

305 previous research of morphological characteristics of digestive gland cells. The EDX analyses

306 indicate elevated amount of tungsten approximately 2.4 wt% in these structures as shown in

307 Table 1.

308

309

310

14

Discussion

311

312   The application of synchrotron based FTIR microspectroscopy to studies of molecular

313   alterations in the digestive gland cells due to ingestion of WO_x nanofibers by model

314   invertebrate organism *P.scaber* have provided new insight into cellular response to nanofibers

315   *in vivo* that can be complemented with the toxicological and cytological results and the

316   inspected surface status of digestive gland epithelium by scanning electron microscopy and

317   energy dispersive X-ray spectrometry.

318   In presented study classical toxicological parameters (weight change, survival and

319   feeding rate) were not affected when animals were exposed to leaves dosed with WO_x

320   nanofiber suspension, providing nominal concentrations of 5000 µg nano-WO_x/g of leaf.

321   After seven days of feeding with nano-WO_x dosed food the stability of the digestive gland cell

322   membrane was affected in almost 20% of animals.

323   The FTIR spectral imaging revealed several significant differences in molecular

324   composition of digestive gland epithelium between control animals and animals exposed to

325   nano-WO_x. Hierarchical cluster analysis of all analysed sections of gland epithelium indicated

326   that the epithelium could be divided into two distinct regions: the central one around the

327   nuclei, and the remainder, which is termed a peripheral region. Since distinct differences

328   between the control and nano-WO_x treated digestive gland epithelium were observed only in

329   the central region, only the central regions will be considered here.

330   The most evident compositional difference between control and WO_x treated samples

331   was found in the lipid to protein ratio. Compared to control cells, the central region of treated

332   cells is enriched in proteins with respect to lipids. This could be interpreted either as increased

333   lipid metabolism due to nano-WO_x ingestion or increased protein synthesis. Since there are no

334   differences in the Amide I and Amide II regions indicating proteins, we assume that the

15

335   difference in the protein/lipid ratio may be attributed to altered lipid metabolism. Similar

336   modifications of lipid/protein ratio have been reported in Gaigneaux et al.,[6] where the authors

337   suggest that an increase of the ratio occurs in multiresistant cells.

338   The methyl to methylene ratio is comparable within the standard deviation of

339   measurements between control and nano-WO_x treated samples, and reveals that the average

340   length and ramification of acyl chains of lipids, and phospholipids in particular, was

341   unaffected by the ingestion of nanofibers. The energies of the methyl and methylene

342   stretching bands are also unaffected. The positions of the signals corresponding to the $=CH_2$

343   and $-CH_3$ moieties provide information regarding the packing characteristics of the acyl

344   chains, which in turn may be related to the fluidity of membrane.[22] Our spectroscopic

345   evidence supports the hypothesis that neither the membrane composition nor structure change

346   as a consequence after nano-WO_x consumption affected membrane fluidity-rigidity. We have

347   not observed any variations in saturation level of lipids but the observed upshift on both vinyl

348   and methine stretching indicates that the unsaturated acyl chains are to a certain extent

349   affected by the ingestion of nanofibers.

350   The FTIR data also show that the carbonyl-to-methyl/methylene ratio (1740/1464 cm$^-$

351   ^{1}) increased upon nanofibers ingestion. Levine et al.[23] and Palaniappan and Pramod[24]

352   interpreted a similar observation as a sign of lipid peroxidation. In our study the downshift

353   and relative increase of the carbonyl band at ~1740 cm^{-1} and the decrease of the

354   methyl/methylene to carbonyl ratio (1464/1400 cm^{-1}) indicates that oxidative processes are

355   taking place. However, we have no indication for changes in the secondary structure of the

356   proteins, which excludes occurrence of protein oxidation.

357   Comparing the results for control and nano-WO_x–treated samples we also found some

358   alterations in the spectral range between 1300 and 1000 cm^{-1}, characteristic for nucleic acids.

16

359   The asymmetric stretching band of the PO_2^- in the backbone of nucleic acids shifts to higher

360   wave numbers upon nano-WO_x ingestion (from 1226 to 1232 cm^{-1}). This trend can be a

361   consequence of a partial reorganization of the nucleic acid structure. Similar FTIR results,

362   shifts from 1225 to 1238 cm^{-1}, were also by Whelan et al.[25] who explain it as an indication of

363   transitions from the B form to the A form of DNA. These authors interpreted this DNA

364   change as a response of different cell types to dehydration. In addition, there are also literature

365   reports suggesting that the B →A transition of DNA might play role in the resistance of DNA

366   to potential damage caused by heat, desiccation and toxic damage.[26]

367   Same as in our study Dovbeshko et al.[27] have also observed changes in spectral range

368   between 1300 and 1000 cm^{-1}.They interpreted asymmetrical stretching vibration (1225 cm^{-1})

369   together with symmetrical stretching vibration (1088 cm^{-1}) in phosphate groups to be a

370   consequence of damage caused to cells by irradiation. That may be related to spatial changes

371   in the positions of the phosphate groups in the RNA helix.

372   In parallel to FTIR and classical toxicity analyses, additional information was

373   provided by SEM inspection of the surface of digestive gland epithelium. In 2 of 8

374   investigated animals, rod like structures containing tungsten have been found, thrust into the

375   apical part of a few epithelial cells. This indicates that the ingested WO_x nanofibers have the

376   potential to interact with individual cells and may result in time in a deleterious effect. This

377   phenomenon has been well studied in the case of asbestos. Wang et al.[28] report asbestos fibres

378   insert into pleural mesothelia cells, inducing chromosomal changes by direct biological or

379   mechanical damage. Similarly, some well knew toxic effect of asbestos nanofibers have also

380   been found in carbon based nanotubes.[2]

381   The FTIR results obtained in our study are in agreement with toxicological and

382   cytological measurements, which indicate that ingestion of nano-WO_x does not affect severely

17

383   the cell membrane stability and feeding behaviour. However, FTIR analyses clearly reveal

384   that the cells are disturbed and respond to the presence of nano-WO_x in the digestive juices.

385   We succeeded to show that ingested WO_x nanofibers activate some cellular

386   mechanisms that may act as a protection against unfavourable conditions. Changed protein to

387   lipid ratio, lipid peroxidation and structural changes of nucleic acids we interpret as responses

388   indicative of non-homeostatic state before oxidative stress and toxic responses are evidenced.

389   To what extend and if at all they are nanoparticle or nanofibres specific is a matter of further

390   research.

391

392   **Author information**

393   **Corresponding author**

394   Phone: + 386 1 423 33. Fax: +386 1 257 33 90. E-mail: damjana.drobne@bf.uni-lj.si

395   **Notes**

396   The authors declare no competing financial interest

397

398

399

400

401

402

18

403   **Tables**

404   **Table 1: EDX elemental composition**

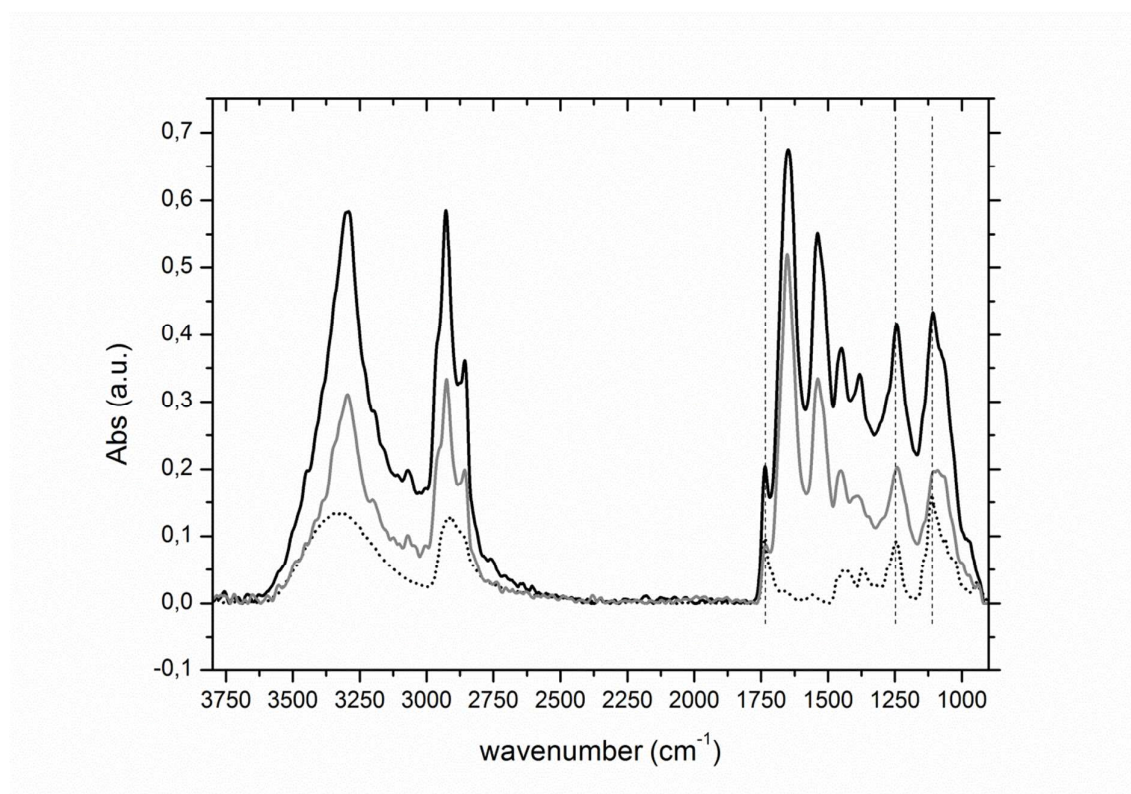| Spectrum	C	O	Ag	W	Os
Spectrum 1	43.32	15.03	5.34	2.40	33.91

405   Table 2: EDX elemental composition of spectrum 1 observed in area showed in Figure 4B.,

406   results in wt.% with some other elements present in cell.

407

408   **Figures**

409

410

19

411   **Figure 1. Spectra of tissue freezing medium used in samples for FTIR analyses.** FTIR

412   spectra of pure tissue freezing medium (dotted spectrum), of a sample point containing a

413   negligible amount of tissue freezing medium (gray spectrum) and a sample point where the

414   tissue freezing medium contribution is clearly visible from the sharp band centred at 1116 cm[-]

415   [1] (black spectrum).
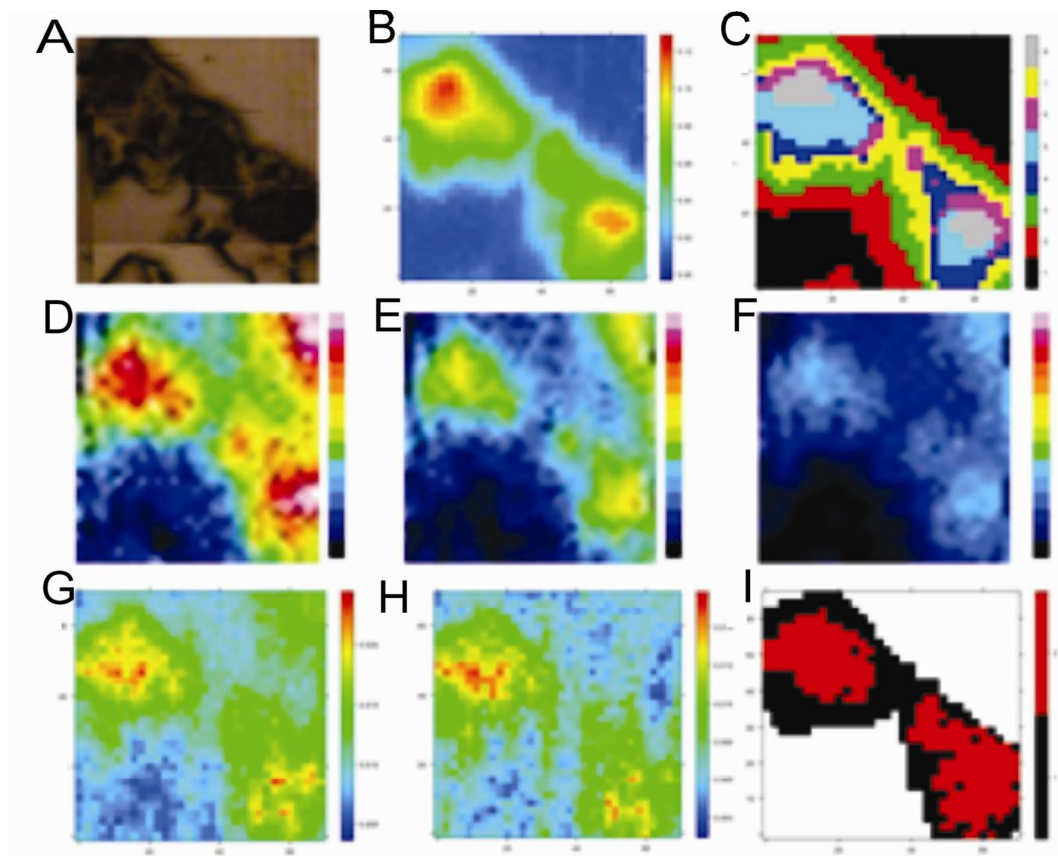
416

417   **Figure 2. The routine steps of chemometric approach in control sample after FTIR**

418   **analyses.** A) Optical image of the control sample K1. B) Chemical FTIR image of the sample

419   obtained integrating the protein spectral region 1720-1480 cm^{-1} (peak area). C) HCA results

420   that show that the tissue freezing medium cluster centroid is the number 1, - the black region

421   outside the sample. D) TFM distribution obtained by integrating the sharp characteristic TFM

422   band centred at 1116 cm^{-1} (peak massif). Clearly, the TFM penetrates the sample. E,F) TFM

423   distribution after the first and second subtraction. G,H) Chemical FTIR image of the sample

20

424   obtained integrating the spectral region of nucleic acids and sugars 1300-900 cm^{-1}, before and

425   after subtraction. The effects of subtraction are particularly clear in the external and peripheral

426   sample regions. The subtraction procedure does not affect the protein or the lipid distribution

427   obtained by integrating the spectral region 3000-2800 cm^{-1} (data not shown). I) Hyperspectral

428   image of the control sample K1 obtained by HCA on vector normalized spectra after TFM

429   subtraction in the spectral region 3000-2800 cm^{-1}.
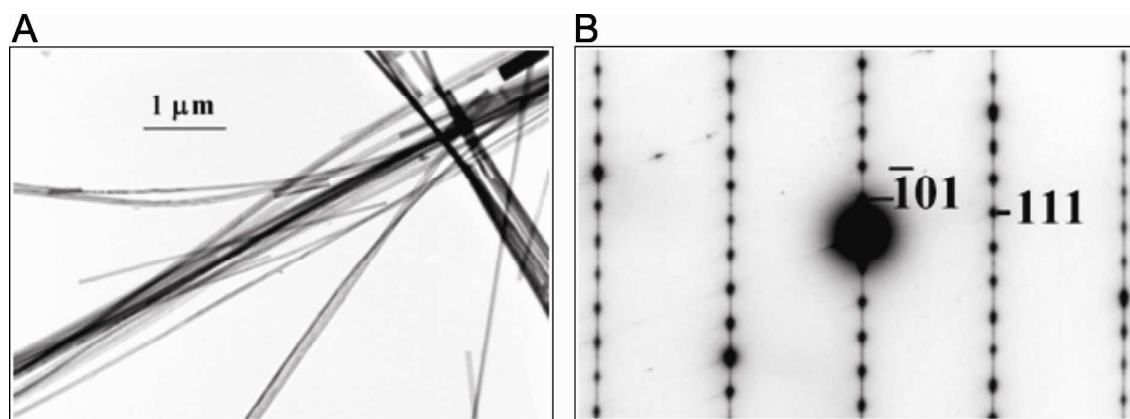

430

431   **Figure 3. Transmission electron microscopy (TEM) of WO$_x$ nanofibers.** A) TEM

432   micrograph of W18O40 nanofibers; B) A diffraction pattern taken on a single fiber showing

433   [1$\bar{2}$1] zone axis.

21

434
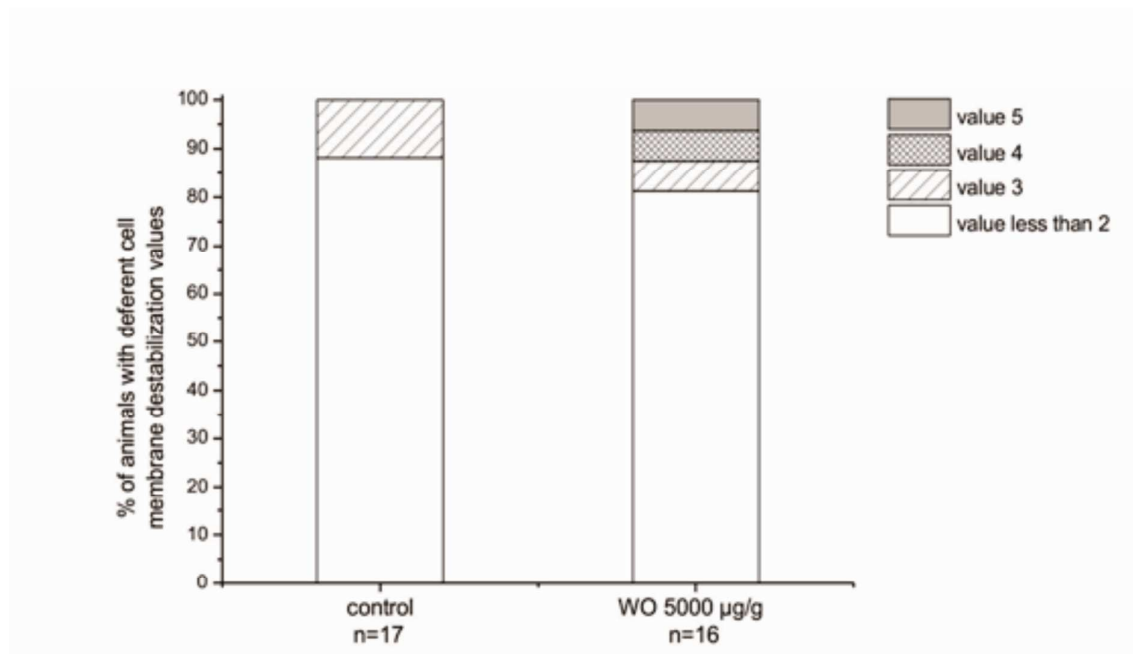
Figure 4. Digestive gland cell membrane stability of control and nano-WO_x exposed

animals. Percentage of animals in each exposed group, with different degrees of destabilised

cell membrane, assessed visually and classified from 0 to 9 according to the predefined scale

as described in Materials and Methods. A digestive gland cell membrane stability value of 2

or less denotes animals which did not have destabilized cell membranes and digestive gland

cell membrane stability values from 3 to 5 animals with destabilized cell membranes. The

value of 5 corresponds to the most highly destabilized cell membranes.

22

442
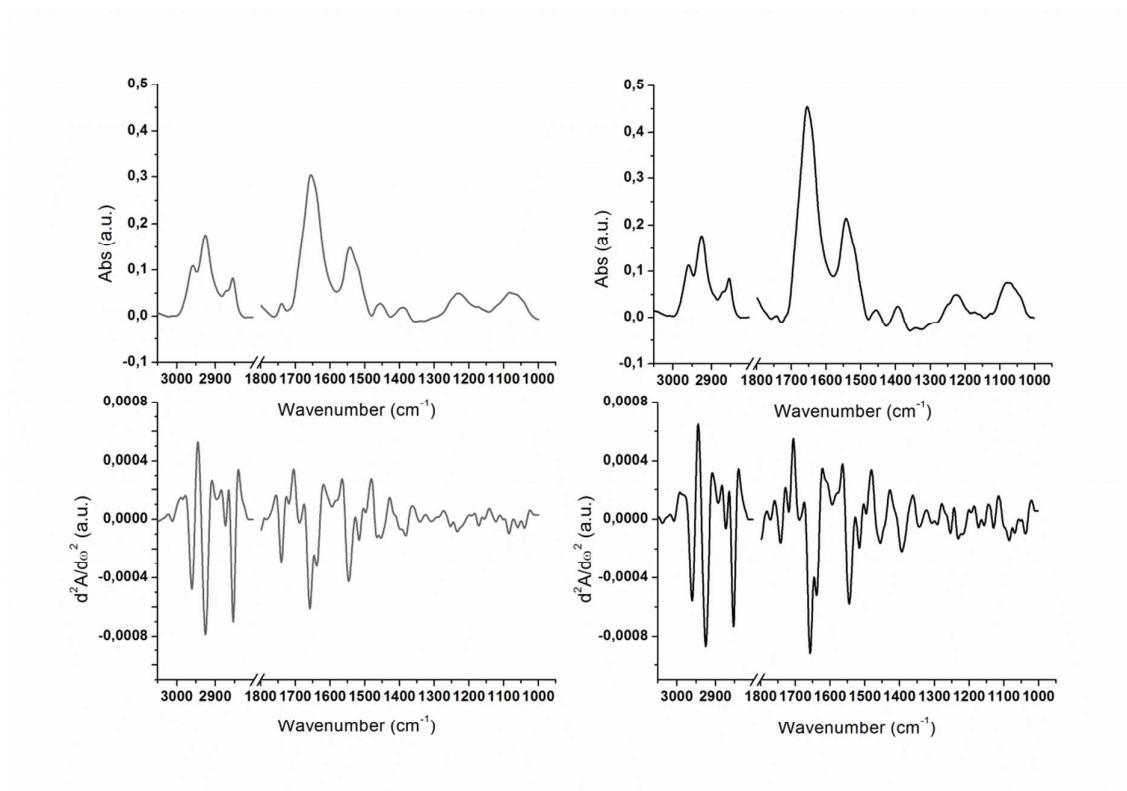
Figure 5. Averge spectras of the central regions of digestive gland tissue. A,B Average spectra of the central regions of WOx treated (grey) and control (black) samples. C,D Second derivative of the average spectra of treated (grey) and control (black) samples, respectively; Savitzky-Golay algorithm, 17 smoothing points).

443

444

445

446

23

447
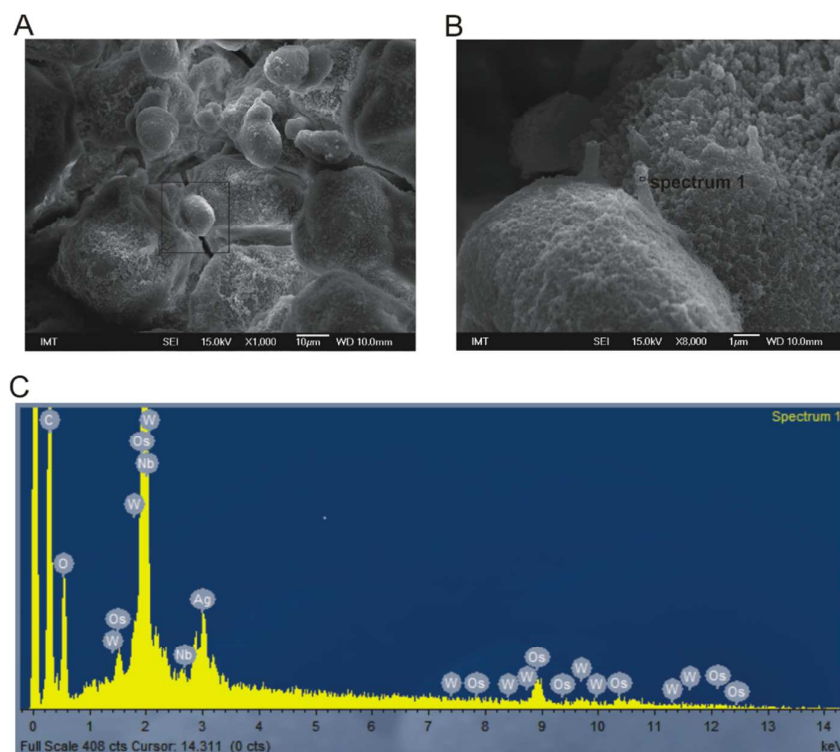
Figure 6. Scanning electron microscopy (SEM) and Energy dispersive x-Ray (EDX) composition of fiber-like structures in digestive gland. Surface of digestive gland epithelium of animal fed with tungsten nanofibers for 7 days with fiber like structures found in one of the cells (A). Digestive gland epithelium cell with thrusted fiber like structures where EDX spectrum was taken (B). EDX spectra of observed area (pointed in figure B) (C).

453

Acknowledgements

24

461   **Supporting Informations**

462   Spectral band assignment where the relevant positions and assignments of the spectral bands

463   are reported and listed in Table S1. In Figure S1 is optical and Fourier transform infrared

464   (FTIR) image of control sample.

465

466   **References**

467   (1)   Lu, X. F.; Liu, X. C.; Zhang, W. J.; Wang, C.; Wei, Y. Large-scale synthesis of

468   tungsten oxide nanofibers by electrospinning. *J. Colloid. Interf. Sci.* **2006,** *298*, (2),

469   996-999.

470   (2)   Jaurand, M. C. F.; Renier, A.; Daubriac, J. Mesothelioma: Do asbestos and carbon

471   nanotubes pose the same health risk? *Part. Fibre. Toxicol.* **2009,** *6*.

472   (3)   Leanderson, P.; Sahle, W. Formation of Hydroxyl Radicals and Toxicity of Tungsten-

473   Oxide Fibers. *Toxicol. in Vitro.* **1995,** *9*, (2), 175-183.

474   (4)   Enriquez, L. S.; Mohammed, T. L. H.; Johnson, G. L.; Lefor, M. J.; Beasley, M. B.

475   Hard metal pneumoconiosis: A case of giant-cell interstitial pneumonitis in a

476   machinist. *Respir. Care.* **2007,** *52*, (2), 196-199.

477   (5)   Lasch, P.; Pacifico, A.; Diem, M. Spatially resolved IR microspectroscopy of single

478   cells. *Biopolymers.* **2002,** *67*, (4-5), 335-338.

479   (6)   Gaigneaux, A.; Ruysschaert, J. M.; Goormaghtigh, E. Infrared spectroscopy as a tool

480   for discrimination between sensitive and multiresistant K562 cells. *Eur. J. Biochem.*

481   **2002,** *269*, (7), 1968-1973.

482   (7)   Karlsson, H. L.; Cronholm, P.; Gustafsson, J.; Moller, L. Copper oxide nanoparticles

483   are highly toxic: A comparison between metal oxide nanoparticles and carbon

484   nanotubes. *Chem. Res. Toxicol.* **2008,** *21*, (9), 1726-1732.

25

485   (8)   Lin, W. S.; Xu, Y.; Huang, C. C.; Ma, Y. F.; Shannon, K. B.; Chen, D. R.; Huang, Y.

486   W. Toxicity of nano- and micro-sized ZnO particles in human lung epithelial cells. *J.*

487   *Nanopart. Res.* **2009,** *11*, (1), 25-39.

488   (9)   Peng, L.; Wenli, D.; Qisui, W.; Xi, L. The envelope damage of Tetrahymena in the

489   presence of TiO2 combined with UV light. *Photochem. Photobiol.* **2010,** *86*, (3), 633-

490   8.

491   (10)   Riding, M. J.; Martin, F. L.; Trevisan, J.; Llabjani, V.; Patel, I. I.; Jones, K. C.;

492   Semple, K. T. Concentration-dependent effects of carbon nanoparticles in gram-

493   negative bacteria determined by infrared spectroscopy with multivariate analysis.

494   *Environ. Pollut.* **2012,** *163*, 226-234.

495   (11)   Saulou, C.; Jamme, F.; Maranges, C.; Fourquaux, I.; Despax, B.; Raynaud, P.; Dumas,

496   P.; Mercier-Bonin, M. Synchrotron FTIR microspectroscopy of the yeast

497   Saccharomyces cerevisiae after exposure to plasma-deposited nanosilver-containing

498   coating. *Anal. Bioanal. Chem.* **2010,** *396*, (4), 1441-1450.

499   (12)   Drobne, D.; Hopkin, S. P. The Toxicity of Zinc to Terrestrial Isopods in a Standard

500   Laboratory Test. *Ecotox. Environ. Safe.* **1995,** *31*, (1), 1-6.

501   (13)   Drobne, D.; Blazic, M.; Van Gestel, C. A. M.; Leser, V.; Zidar, P.; Jemec, A.; Trebse,

502   P. Toxicity of imidacloprid to the terrestrial isopod Porcellio scaber (Isopoda,

503   Crustacea). *Chemosphere.* **2008,** *71*, (7), 1326-1334.

504   (14)   Remskar, M.; Kovac, J.; Virsek, M.; Mrak, M.; Jesih, A.; Seabaugh, A. W5O14

505   nanowires. *Adv. Funct. Mater.* **2007,** *17*, (12), 1974-1978.

506   (15)   Valant, J.; Drobne, D.; Sepcic, K.; Jemec, A.; Kogej, K.; Kostanjsek, R. Hazardous

507   potential of manufactured nanoparticles identified by in vivo assay. *J. Hazard. Mater.*

508   **2009,** *171*, (1-3), 160-165.

509   (16)   Lupi, S.; Nucara, A.; Perucchi, A.; Calvani, P.; Ortolani, M.; Quaroni, L.; Kiskinova,

510   M. Performance of SISSI, the infrared beamline of the ELETTRA storage ring. *J. Opt.*

511   *Soc. Am. B.* **2007,** *24*, (4), 959-964.

512   (17)   Liao, C.; Piercey-Normore, M. D.; Sorensen, J. L.; Gough, K. In situ imaging of usnic

513   acid in selected Cladonia spp. by vibrational spectroscopy. *Analyst.* **2010,** *135*, (12),

514   3242-3248.

515   (18)   Stitt, D. M.; Kastyak-Ibrahim, M. Z.; Liao, C. R.; Morrison, J.; Albensi, B. C.; Gough,

516   K. M. Tissue acquisition and storage associated oxidation considerations for FTIR

517   microspectroscopic imaging of polyunsaturated fatty acids. *Vib. Spectrosc.* **2012,** *60*,

518   16-22.

519   (19)   Beleites, C.; Sergo, V. HyperSpec: A Package to Handle Hyperspectral Data Sets in R.

520   **2012**.

521   (20)   Beleites, C.; Neugebauer, U.; Bocklitz, T.; Krafft, C.; Popp, J. Sample size planning

522   for classification models. *Anal. Chim. Acta.* **2013,** *760*, 25-33.

523   (21)   Leser, V.; Drobne, D.; Pipan, Z.; Milani, M.; Tatti, F. Comparison of different

524   preparation methods of biological samples for FIB milling and SEM investigation. *J.*

525   *Microsc.* **2009,** *233*, (2), 309-19.

526   (22)   Jackson, M.; Mantsch, H.H. The Use and Misuse of Ftir Spectroscopy in the

527   Determination of Protein-Structure. *Crit. Rev. Biochem. Mol.* **1995**, *30*, 95-120.

528   (23)   LeVine, S.M.; Wetzel, D.L. Chemical analysis of multiple sclerosis lesions by FT-IR

529   microspectroscopy. *Free. Radical. Bio. Med.* **1998**, *25*, 33-41.

530   (24)   Palaniappan, P. R.; Pramod, K. S. FTIR study of the effect of nTiO(2) on the

531   biochemical constituents of gill tissues of Zebrafish (Danio rerio). *Food. Chem.*

532   *Toxicol.* **2010,** *48*, (8-9), 2337-2343.

533   (25)   Whelan, D. R.; Bambery, K. R.; Heraud, P.; Tobin, M. J.; Diem, M.; McNaughton, D.;

534   Wood, B. R. Monitoring the reversible B to A-like transition of DNA in eukaryotic

535   cells using Fourier transform infrared spectroscopy. *Nucleic. Acids. Res.* **2011,** *39*,

536   (13), 5439-5448.

537   (26)   Lee, K. S.; Bumbaca, D.; Kosman, J.; Setlow, P.; Jedrzejas, M. J. Structure of a

538   protein-DNA complex essential for DNA protection in spores of Bacillus species. *P.*

539   *Natl. Acad. Sci. USA.* **2008,** *105*, (8), 2806-2811.

540   (27)   Dovbeshko, G. I.; Gridina, N. Y.; Kruglova, E. B.; Pashchuk, O. P. FTIR spectroscopy

541   studies of nucleic acid damage. *Talanta.* **2000,** *53*, (1), 233-246.

542   (28)   Wang, N. S.; Jaurand, M. C.; Magne, L.; Kheuang, L.; Pinchon, M. C.; Bignon, J. The

543   Interactions between Asbestos Fibers and Metaphase Chromosomes of Rat Pleural

544   Mesothelial Cells in Culture - a Scanning and Transmission Electron-Microscopic

545   Study. *Am. J. Pathol.* **1987,** *126*, (2), 343-349.

546